INSTITUTE OF MATHEMATICS

THE CZECH ACADEMY OF SCIENCES

Multiscale simulation of dilute polymer solutions

Hana Mizerová
Bangwei She

Preprint No. 104-2017

PRAHA 2017

Multiscale simulation of dilute polymer solutions

Hana Mizerová* and Bangwei She†

Institute of Mathematics, Czech Academy of Sciences, Žitná 25, 11567 Prague 1, Czech Republic

Abstract

We propose a conservative multiscale scheme for the numerical simulation of a high-dimensional Navier-Stokes-Fokker-Planck system for dilute polymer solutions. The incompressible Navier-Stokes equations model the unsteady motion of the Newtonian solvent, while the Fokker-Planck equation describes the evolution of the probability density function of infinitely extensible polymer dumbbell molecules. This leads to a problem of unbounded domain. Our method combines a Lagrange-Galerkin and a Hermite spectral methods together with a space splitting approach. We prove theoretically that the proposed scheme satisfies the discrete conservation of mass with respect to the probability density. Several numerical experiments are presented to illustrate the performance of the solver, and to confirm the conservation of mass at the discrete level.

Keywords: stabilized Lagrange-Galerkin; Hermite spectral method; unbounded domain; mass conservative scheme; space splitting; viscoelastic fluids; Navier-Stokes-Fokker-Planck; kinetic dumbbell theory; Oldroyd-B model; Peterlin model

1 Introduction

In everyday life we encounter a huge class of multi-component fluids displaying non-Newtonian behaviour due to their underlying micro-structure and its interaction with solvent. Examples of such complex fluids are polymeric melts, solutions, biopolymers (DNA, proteins), and also known from daily life such as blood, glue, and detergent. We deal with a multiscale simulation of a class of models arising as microscopic-macroscopic bead-spring models from the kinetic theory of dilute polymer solutions with non-interacting polymeric chains.

The kinetic model considered in the present paper is a Navier-Stokes-Fokker-Planck system describing the unsteady motion of viscoelastic fluids with infinitely

*mizerova@math.cas.cz

†she@math.cas.cz

extensible molecular chains. This leads to a challenging problem of numerical solution in an unbounded domain in a configuration space of polymer molecules.

The simplest model of our current interest is the Hookean dumbbell model that corresponds to a linear spring force law for the bead-spring models of dilute polymer solutions. Recently, Barrett and Süli in [3], along the side of the proof of existence of global-in-time large-data weak solutions, rigorously showed that the well-known Oldroyd-B model is indeed the macroscopic closure of the Hookean dumbbell model. Let us mention that, generally, the macroscopic closure of kinetic models with nonlinear spring force is not possible unless we approximate the nonlinear spring function. We consider the Peterlin approximation which replaces the length of polymer molecules in the spring coefficient by the average length, cf. [21]. We would like to point out that the averaging in the nonlinear spring function results in the additional coefficients appearing in the Fokker-Planck equation. They depend on the average length of polymer molecules that is a macroscopic quantity only, namely the trace of the conformation tensor $\operatorname{tr}\mathbf{C} = \langle|\mathbf{R}|^2\rangle$. In the recent work [9] the macroscopic closure of the proposed kinetic Peterlin model allowed us to study the existence of global-in-time weak solutions. Note that the macroscopic counterpart of the proposed kinetic model is the (macroscopic) Peterlin viscoelastic model that has been studied in our previous work both from the theoretical and numerical point of view, see [14–16].

Let us mention that for a multiscale simulation of kinetic viscoelastic models confined to a bounded domain both in the physical and the configuration space we can already find several results in the literature. For instance, the most commonly studied kinetic dumbbell-based model is the FENE model (finitely extensible nonlinear elastic), in which a particular form of the corresponding nonlinear spring potential restricts the system of equations to a bounded domain, see, e.g., [1, 5, 11, 13]. Another example is the Doi model with rod-like molecules of finite length, cf. [10]. However, the methods developed for bounded domains can not, in general, be efficiently extended to the case of infinite configuration space. Let us emphasize that the Peterlin approximation of the spring force does not provide finite extensibility of polymeric chains, and therefore we have to deal with the problem of an unbounded domain. To the best of our knowledge there are no available multiscale simulation methods for dilute polymer solutions with infinitely extensible molecules.

1.1 The Navier-Stokes-Fokker-Planck system

Widely studied models of polymeric fluids represent them simply as chains of beads and springs or beads and rods surrounded by a Newtonian fluid. In our case the solvent confined to a bounded domain $\Omega \subset \mathbb{R}^d$, $d = 2, 3$, is described by the incompressible Navier-Stokes equations

$$\frac{\partial \mathbf{u}}{\partial t} + \mathbf{u}\cdot\nabla\mathbf{u} = -\nabla p + 2\nu\nabla\cdot\mathbf{D}(\mathbf{u}) + \nabla\cdot\mathbf{T}, \quad \nabla\cdot\mathbf{u} = 0. \tag{1a}$$

Here the couple $(\mathbf{u}, p) : \Omega \times (0, T) \to \mathbb{R}^d \times \mathbb{R}$ denotes the velocity and pressure, ν stands for the solvent viscosity. The symmetric part of the velocity gradient

is given by $\mathbf{D}(\mathbf{u}) := (\nabla\mathbf{u} + (\nabla\mathbf{u})^T)/2$. Each end-to-end dumbbell molecule is represented by its orientation vector $\mathbf{R}$ that belongs to the configuration space $\mathfrak{D} := \mathbb{R}^d$. The probability density function $\psi : \Omega \times \mathfrak{D} \times (0,T) \to \mathbb{R}$ gives the probability of a dumbbell that it stays between $\mathbf{R}$ and $(\mathbf{R} + d\mathbf{R})$ in space $\mathfrak{D}$, at a physical point $\mathbf{x} \in \Omega$ and time $t \in [0,T]$. It satisfies the following Fokker-Planck equation

$$\frac{\partial\psi}{\partial t} + \mathbf{u}\cdot\nabla_x\psi - \varepsilon\Delta_x\psi = -\nabla_R\cdot\big(\nabla_x\mathbf{u}\cdot\mathbf{R}\big) + \frac{\Gamma(\mathrm{tr}\mathbf{C})}{2\lambda}\Big(\nabla_R\cdot\big(\mathbf{R}\psi\big) + \Delta_R\psi\Big). \tag{1b}$$

Note that

$$\int_{\mathfrak{D}} \psi(t,\mathbf{x},\mathbf{R})\, d\mathbf{R} = 1, \quad \forall (t,\mathbf{x}) \in [0,T]\times\Omega. \tag{1c}$$

The system is equipped with the decay/boundary and initial conditions,

$$\psi|_{|\mathbf{R}|\to\infty} = 0, \quad \frac{\partial\psi}{\partial\mathbf{n}}|_{\partial\Omega} = \mathbf{0}, \qquad \mathbf{u}|_{\partial\Omega} = \mathbf{0}, \tag{1d}$$

$$\psi(0) = \psi^0, \qquad \mathbf{u}(0) = \mathbf{u}^0, \tag{1e}$$

where $\mathbf{u}_0 : \Omega \to \mathbb{R}^d$, $\psi_0 : \Omega\times\mathfrak{D} \to \mathbb{R}$ are suitable initial functions with ψ^0 satisfying (1c). The elastic stress tensor $\mathbf{T} : \Omega \times (0,T) \to \mathbb{R}^{d\times d}$ is appearing in (1a) as a forcing term on the right-hand side of the momentum equation due to the random movement of polymer molecules. It is obtained by means of Kramer's expression,

$$\mathbf{T} = \gamma(\mathrm{tr}\mathbf{C})\mathbf{C} - \mathbf{I}. \tag{1f}$$

where $\mathbf{C} : \Omega \times (0,T) \to \mathbb{R}^{d\times d}$, given by

$$\mathbf{C} := \int_{\mathbb{R}^d} (\mathbf{R}\otimes\mathbf{R})\psi(t,\mathbf{x},\mathbf{R})\, d\mathbf{R}, \tag{1g}$$

is the symmetric positive definite conformation tensor. Functions $\Gamma, \gamma \in C(\mathbb{R}^+;\mathbb{R})$ appearing in (1b) and (1f) due to the Peterlin approximation depend on the structure parameter $\mathrm{tr}\,\mathbf{C} := \sum_i C_{ii} > 0$. They will be specified later based on the fluid model chosen in the numerical experiments. The positive constants ε and λ stand for the centre-of-mass diffusion coefficient and the Deborah number describing the elastic relaxation property of the polymer dumbbells, respectively. As already mentioned above, the Peterlin approximation allows the macroscopic closure of the Fokker-Planck equation (1b) which yields a partial differential equation for $\mathbf{C}$. *Formal* integration of (1b) multiplied by $\mathbf{R}\otimes\mathbf{R}$ over the configuration space $\mathfrak{D}$ yields

$$\frac{\partial\mathbf{C}}{\partial t} + (\mathbf{u}\cdot\nabla_x)\mathbf{C} - \varepsilon\Delta_x\mathbf{C} = -(\nabla_x\mathbf{u})\mathbf{C} - \mathbf{C}(\nabla_x\mathbf{u})^T + \frac{\Gamma(\mathrm{tr}\mathbf{C})}{2\lambda}\big(\mathbf{C}-\mathbf{I}\big). \tag{2}$$

Equation (2) is then equipped with the corresponding Neumann boundary condition, $\nabla_x\mathbf{C}\cdot\mathbf{n} = \mathbf{0}$, and initial condition $\mathbf{C}(0) = \mathbf{C}^0$. Note that throughout the paper we might omit the dependence of functions on the variables $t, \mathbf{x}, \mathbf{R}$ when there is no confusion.

Definition 1. *We refer the system of equations* (1) *as the* kinetic Peterlin model, *while the system of equations* (1a), (1f), (1g) *and* (2) *together with the boundary and initial conditions for the couple* $(\mathbf{u}, \mathbf{C})$ *as the* Peterlin viscoelastic model.

Remark 1. *As already pointed out in [9], the standard derivations of bead-spring models routinely omit the diffusive term appearing in the Fokker-Planck equation and, consequently, also in the corresponding macroscopic equation for the elastic stress. However, in [2, 7, 24] it has been shown that the diffusion has indeed a physical rationale. Therefore we consider the center-of-mass diffusion in* (1b) *and hence also in* (2) *with a small constant* $\varepsilon \geq 0$.

The above introduced Peterlin viscoelastic model covers a large class of macroscopic models of viscoelastic fluids, cf. [14] and the references therein. For instance, setting both γ and Γ constant we get the well-known Oldroyd-B model (for $\varepsilon > 0$ its diffusive version). For $\varepsilon = 0$, arbitrary Γ and constant γ we obtain the PTT model.

The rest of the paper is organized as follows. In Section 2 we propose the numerical method and prove that our scheme is, at the discrete level, mass preserving with respect to the probability density function ψ. Section 3 contains several numerical examples to validate the method.

2 Numerical method

In this section we derive a multiscale method for the Navier-Stoke-Fokker-Planck system (1) as a coupling of two solvers: one for the macroscopic solvent and the other for the high-dimesional molecular part. More precisely, we approximate the Navier-Stokes equations by a stabilized Lagrange-Galerkin method, and apply a space splitting method on the Fokker-Planck equation. The part corresponding to the infinite configuration space will be solved by means of a Hermite spectral method, and the other part corresponding to the finite physical space will be again solved by the Lagrange-Galerkin method.

2.1 Lagrange-Galerkin method

Firstly, we discretize the time interval $[0, T]$ into N_T equidistant parts, and denote by $t^n = n\Delta t$ for $n = 0, 1, \cdots, N_T$ the current time step, and by $\Delta t = \frac{T}{N_T}$ the fixed time increment.

In what follows we briefly explain the Lagrange-Galerkin method (LG) introduced in [20] to approximate the Navier-Stokes equations. This method employs the following first-order approximation of the material derivative $\mathrm{D}\mathbf{g}/\mathrm{Dt}$ of a function $\mathbf{g} : \Omega \times [0, T] \to \mathbb{R}^l$, $l \in \{1, 2\}$,

$$\frac{\mathrm{D}\mathbf{g}}{\mathrm{D}t}(\mathbf{x}, t^n) := \left(\frac{\partial \mathbf{g}}{\partial t} + (\mathbf{u} \cdot \nabla_x)\mathbf{g}\right)(\mathbf{x}, t^n) = \frac{\mathbf{g}^n(\mathbf{x}) - \left(\mathbf{g}^{n-1} \circ X_1^n\right)(\mathbf{x})}{\Delta t} + O(\Delta t), \quad (3)$$

where $X_1^n : \Omega \to \mathbb{R}^d$ is a mapping defined by $X_1^n(\mathbf{x}) := \mathbf{x} - \mathbf{u}^n(\mathbf{x})\Delta t$. The symbol $\circ$ means the composition of functions, $(\mathbf{g}^{n-1} \circ X_1^n)(x) := \mathbf{g}^{n-1}(X_1^n(x))$ with $\mathbf{g}^n(\mathbf{x}) := \mathbf{g}(t^n, \mathbf{x})$. Approximation (3) following the characteristics of particles backward in time has appeared as a powerful tool for numerical solution of equations describing viscoelastic fluids, for which not only the current state but also the history of motion is important.

Let Ω be a polygonal domain, $\mathcal{T}_h := \{K\}$ a triangulation of $\bar{\Omega} := \bigcup_{K \in \mathcal{T}_h} K$, h_K the diameter of $K \in \mathcal{T}_h$, $h := \max_{K \in \mathcal{T}_h} h_K$ the maximum element size, and $\mathcal{V}_h$ the set of all vertices $\mathbf{x}_i$ in $\mathcal{T}_h$. We consider a regular family of subdivisions $\{\mathcal{T}_h\}_{h \downarrow 0}$ satisfying the inverse assumption [6]. We consider a conforming finite element approximation of the velocity and pressure satisfying the Navier-Stokes equations (1a), and the probability density function satisfying the part of the Fokker-Planck equation corresponding to the physical space, see (5) below. To this end we define the following discrete finite element spaces

$$X_h^d := \{\mathbf{v}_h \in C^0(\bar{\Omega}_h)^d; \mathbf{v}_h|_K \in \mathcal{P}^1(K)^d, \forall K \in \mathcal{T}_h\},$$
$$V_h := X_h^d \cap V, \; W_h := X_h^1 \cap H^1(\Omega), \; Q_h := X_h^1 \cap Q,$$

where $V := H^1_{0,\sigma}(\Omega)^2$, $Q := L^2_0(\Omega)$ are the classical functions spaces, and $\mathcal{P}^1(K)$ is the polynomial space of linear functions on element K. It is well-known that the $\mathcal{P}^1/\mathcal{P}^1$-approximation of the couple $(\mathbf{u}, p)$ solving (1a) does not satisfy the inf-sup condition. Therefore we employ the Brezzi-Pitkaränta pressure stabilization [4], see (19) below. For more details on LG we refer the reader to [19, 20] or our previous work [15–17], where the above described method has been successfully employed for the numerical simulation of macroscopic viscoelastic models.

2.2 Space splitting for the Fokker-Planck equation

We adopt the space splitting method, also called alternating-direction method, that has been applied for FENE model by Lozinski and Chauviere in [5], and Knezevic and Süli in [11]. Since the Fokker-Planck equation involves both the configuration space ($\mathbf{R} \in \mathfrak{D} = \mathbb{R}^d$) and the physical space ($\mathbf{x} \in \Omega \subset \mathbb{R}^d$), it is natural for the numerical simulation to decompose equation (1b) into two parts accordingly. For the approximation of the Fokker-Planck equation in the configuration space we adopt the Hermite spectral method, which is naturally designed for an unbounded domain, cf. [8]. To solve the equation in the physical space we use the LG method described in Subsection 2.1. Consequently, we solve two systems of equations in two sub-spaces.

Definition 2. (Space splitting)
Firstly, we fix a point in the physical space $\mathbf{x} \in \Omega$ *and solve the first part of* (1b) *in the configuration space* $\mathfrak{D} := \mathbb{R}^2$,

$$\frac{\psi^* - \psi^n}{\Delta t} = \nabla_R \cdot ((-\nabla_x \mathbf{u}^n \cdot \mathbf{R} + \xi \mathbf{R})\psi^*) + \chi \Delta_R \psi^*, \quad \mathbf{R} \in \mathfrak{D}. \tag{4}$$

In the second step we fix the point in the configuration space $\mathbf{R} \in \mathfrak{D}$ *and solve the rest of* (1b) *in the physical space,*

$$\frac{\psi^{n+1} - \psi^*}{\Delta t} - \mathbf{u}^n \cdot \nabla_x \psi^* - \varepsilon \Delta_x \psi^{n+1} = 0, \quad \mathbf{x} \in \Omega. \tag{5}$$

2.3 Hermite spectral method for an unbounded domain

In order to deal with the problem of infinite configuration space we consider a spectral method based on the weighted Hermite polynomials. Due to their useful properties, they have been already used to derive numerical methods for problems on unbounded domains. The readers are invited to read, for instance, [8, 23].

Before we derive the spectral method, let us introduce the definition and useful properties of the *Weighted Hermite polynomial [18]*. It is defined for $r \in \mathbb{R}$ as

$$\tilde{H}_m(r) := \frac{\omega_\alpha}{\sqrt{2^m m!}} H_m(\alpha r), \ \omega_\alpha(r) := e^{\alpha^2 r^2}, \ \alpha > 0, \ m \geq 0, \tag{6}$$

where the Hermite polynomial of degree m is defined as

$$H_m(r) := (-1)^m e^{r^2} \partial_r^m (e^{-r^2}), \ r \in \mathbb{R}. \tag{7}$$

The weighted Hermite polynomials are orthogonal with respect to the weight ω_α,

$$\int_{\mathbb{R}} \tilde{H}_m(r) \tilde{H}_n(r) \omega_\alpha(r) = \frac{\sqrt{\pi}}{\alpha} \delta_{mn}, \tag{8}$$

δ_{mn} being the Kronecker delta. Moreover, they satisfy the following properties that shall be used for the derivation of the configuration space solver (15) below

$$\alpha r \tilde{H}_m(r) = \sqrt{\frac{m+1}{2}} \tilde{H}_{m+1}(r) + \sqrt{\frac{m}{2}} \tilde{H}_{m-1}(r), \tag{9a}$$

$$\frac{d}{dr} \tilde{H}_m(r) = -\alpha \sqrt{2(m+1)} \tilde{H}_{m+1}(r), \tag{9b}$$

$$r \frac{d}{dr} \tilde{H}_m(r) = -\sqrt{(m+1)(m+2)} \tilde{H}_{m+2}(r) - (m+1) \tilde{H}_m(r), \tag{9c}$$

$$\frac{d^2}{dr^2} \tilde{H}_m(r) = 2\alpha^2 \sqrt{2(m+1)(m+2)} \tilde{H}_{m+2}(r). \tag{9d}$$

Another useful feature of this function is

$$\tilde{H}_m(r) \longrightarrow 0 \text{ as } r \longrightarrow \infty. \tag{10}$$

We refer the reader to, e.g., [8, 22, 25] and the references therein for the definition, and an overview of the properties of the weighted Hermite polynomials.

For the simplicity of notation and better readability let us fix the dimension in what follows to $d = 2$. Note that the method can be analogously derived for $d = 3$. Let $\mathbf{R} := (r_1, r_2) \in \mathfrak{D} = \mathbb{R}^2$. We define a grid point $\mathbf{R}_{ij} := (r_{1,i}, r_{2,j})$, where

$r_{1,i}$ and $r_{2,j}$ are the roots of the Hermite polynomial $H_{N+1}(r)$. Consequently, we can define the mesh $\mathfrak{D}_N$ as the set of $(N+1)\times(N+1)$ grid points $\mathbf{R}_{ij}$, i.e.,

$$\mathfrak{D}_N := \big\{\mathbf{R}_{ij} = (r_{1,i}, r_{2,j}),\, i,j = 0,1,\cdots,N;\, H_{N+1}(r_{1,i}) = H_{N+1}(r_{2,j}) = 0\big\}. \quad (11)$$

To solve the Fokker-Planck equation (1b) we use the spectral method based on the weighted Hermite polynomials introduced above. To this end we define the space $\mathcal{P}_N := \text{span}\,\{\tilde{H}_m(r)\}_{m=0}^N$, and $\mathcal{P}_N^2 := \mathcal{P}_N \otimes \mathcal{P}_N$. We seek an approximate solution $\psi_{h,N} \in W_h \otimes \mathcal{P}_N^2$ in the form

$$\psi_{h,N}^n(\mathbf{x},\mathbf{R}) = \sum_{i=0}^N \sum_{j=0}^N \phi_{ij}^n(\mathbf{x})\, \tilde{H}_i(r_1)\tilde{H}_j(r_2),\ \forall t^n,\ n = 0,\ldots,N_T. \quad (12)$$

Note that property (10) together with the above defined spectral decomposition of the approximate solution directly imply that the decay boundary condition in (1d) is satisfied at the discrete level.

In order to get the macroscopic quantities from the probability density functions we need to compute integrals over the infinite configuration space. To this end we use the Hermite-Gauss quadrature.

Theorem 2.1. [22, Theorem 7.3] (Hermite-Gauss quadrature)
Let $\{r_i\}_{i=0}^N$ be the zeros of $H_{N+1}(r)$, and $\{w_i\}_{i=0}^N$ be the weights given by

$$w_i := \frac{2^N\sqrt{\pi}N!}{(N+1)H_N^2(r_i)}, \quad 0 \le i \le N.$$

Then,

$$\int_{\mathbb{R}} p(r)\mathrm{e}^{-r^2}\,dr = \sum_{i=0}^N p(r_i)w_i, \quad p \in \mathcal{P}^{2N+1}(\mathbb{R}). \quad (13)$$

For instance, we get the discrete value of the off-diagonal component of conformation tensor from the approximation $\psi_{h,N}$ given by (12) as follows

$$\begin{aligned} C_{12} = C_{21} &= \int_{\mathbb{R}}\int_{\mathbb{R}} r_1 r_2\, \psi_{h,N}(r_1,r_2)\,dr_1\,dr_2 \\ &= \sum_{i=0}^N \sum_{j=0}^N \phi_{ij}^n \int_{\mathbb{R}} r_1\tilde{H}_i(r_1)\,dr_1 \int_{\mathbb{R}} r_2\tilde{H}_j(r_2)\,dr_2. \end{aligned} \quad (14)$$

The two integrals in (14) are then computed by (13) for $p(r) = r\tilde{H}_i(r)\,\mathrm{e}^{r^2} \in C^\infty(\mathbb{R})$.

Configuration space solver We insert (12) into equation (4), multiply it with the test function $\tilde{H}_z(r_1)\tilde{H}_k(r_2)\omega_\alpha(r_1)\omega_\alpha(r_2)$, and integrate over the configuration space $\mathfrak{D}$. After employing the orthogonality (8) and the properties (9) of the weighted Hermite polynomials we obtain the following *finite difference* scheme:

$$\frac{\phi_{zk}^* - \phi_{zk}^n}{\Delta t}(\mathbf{x}_i) = \mathbb{L}(\phi_{zk}^*(\mathbf{x}_i)), \quad \mathbf{x}_i \in \mathcal{V}_h, \quad z,k = 0,\ldots,N, \quad (15)$$

where

$$\begin{aligned}\mathbb{L}(\phi_{zk}) := {} & \phi_{z-2,k}(2\alpha^2\gamma_2 - A_{11})\sqrt{z(z-1)} + \phi_{z-1,k-1}(-A_{12} - A_{21})\sqrt{zk} \\ & + \phi_{z-1,k+1}(-A_{12})\sqrt{z(k+1)} + \phi_{z,k-2}(2\alpha^2\gamma_2 - A_{22})\sqrt{k(k-1)} \\ & + \phi_{z,k}(-A_{11}z - A_{22}k) + \phi_{z+1,k-1}(-A_{12})\sqrt{(z+1)k}.\end{aligned} \tag{16}$$

Note that $\phi_{z,k} \equiv 0$ if any of z, k is less than 0 or grater than N.

Physical space solver We insert (12) into (5), multiply it with the test function $\tilde{H}_z(r_1)\tilde{H}_k(r_2)\omega_\alpha(r_1)\omega_\alpha(r_2)\varphi_h$, and integrate over both the configuration space $\mathfrak{D}$ and the physical domain Ω. Consequently, using the LG method introduced in Subsection 2.1 we derive an equation for the unknowns ϕ^n_{zk}. It reads

$$\left(\frac{\phi^{n+1}_{zk} - \phi^*_{zk} \circ X^n_1}{\Delta t}, \varphi_h\right) + \varepsilon(\nabla_x \phi^{n+1}_{zk}, \nabla_x \varphi_h) = 0, \quad z, k = 0, \ldots, N. \tag{17}$$

2.4 Multiscale method

We now formulate our multiscale method for the numerical solution of the Navier-Stoke-Fokker-Planck system (1) for dilute solutions with infinitely extensible polymer molecules.

Definition 3. (multiscale scheme)
Let $\mathbf{u}^0_h \in V_h$ and $\psi^0_{h,N} \in X^1_h \times \mathcal{P}^2_N$ be the initial values. We seek a solution $\{\mathbf{u}^{n+1}_h, p^{n+1}_h, \phi^{n+1}_{zk}\}_{n=0}^{N_T-1} \subset V_h \times Q_h \times W_h$ satisfying

$$\frac{\phi^*_{zk}(\mathbf{x}_i) - \phi^n_{zk}(\mathbf{x}_i)}{\Delta t} = \mathbb{L}(\phi^*_{zk}(\mathbf{x}_i)) \quad \text{for } z, k = 0, \ldots, N \text{ and a fixed } \mathbf{x}_i \in \mathcal{V}_h, \tag{18a}$$

$$\left(\frac{\phi^{n+1}_{zk} - \phi^*_{zk} \circ X^n_1}{\Delta t}, \varphi_h\right) + \varepsilon(\nabla_x \phi^{n+1}_{zk}, \nabla_x \varphi_h) = 0 \quad \text{in } \Omega_h \text{ for fixed } z, k, \tag{18b}$$

$$\begin{aligned}\left(\frac{\mathbf{u}^{n+1}_h - \mathbf{u}^n_h \circ X^n_1}{\Delta t}, \mathbf{v}_h\right) + 2\nu\left(\mathbf{D}(\mathbf{u}^{n+1}_h), \mathbf{D}(\mathbf{v}_h)\right) - (p^{n+1}_h, \nabla_x \cdot \mathbf{v}_h) - (\nabla_x \cdot \mathbf{u}^{n+1}_h, q_h) \\ + \mathcal{S}_h(p^{n+1}_h, q_h) = \left(\mathbf{T}^{n+1}_h, \nabla_x \mathbf{v}_h\right) \quad \text{in } \Omega_h,\end{aligned} \tag{18c}$$

for any test function $(\mathbf{v}_h, q_h, \varphi_h) \in V_h \times Q_h \times W_h$. Here the pressure stabilization term is given by

$$\mathcal{S}_h(p_h, q_h) := \delta_0 \sum_K h^2_K \nabla p_h \nabla q_h, \tag{19}$$

where $\delta_0 > 0$ is constant. The piecewise linear continuous approximation $\mathbf{T}^{n+1}_h$ is obtained by the interpolation of the discrete values $\mathbf{T}^{n+1}(\mathbf{x}_i) = \mathbf{T}(\psi^{n+1}_{h,N}(\mathbf{x}_i, \mathbf{R}_{lj}))$ that are computed by Kramer's expression (1f) and Hermite-Gauss quadrature. Here the approximate solution $\psi^{n+1}_{h,N} \in W_h \times \mathcal{P}^2_N$ is computed from the solution $\phi^{n+1}_{zk}(\mathbf{x}_i)$ of equations (18a)-(18b) by

$$\psi^{n+1}_{h,N}(\mathbf{x}_i, \mathbf{R}_{lj}) = \sum_{z=0}^{N}\sum_{k=0}^{N} \phi^{n+1}_{zk}(\mathbf{x}_i)\, \tilde{H}_z(r_{1,l})\tilde{H}_k(r_{2,j}), \quad \text{for } \mathbf{x}_i \in \mathcal{V}_h \text{ and } \mathbf{R}_{lj} \in \mathfrak{D}_N.$$

Remark 2. *In all numerical tests in Section 3 we set the stabilization constant in (19) to be $\delta_0 = 0.05$. Note that the multiscale scheme (18) has no requirements on the time step Δt. Indeed, the Lagrange-Galerkin method in (18c), (18b) has no limitation on the time step due to the discretization of material derivative along the trajectory curve. The Hermite spectral method (18a) neither needs a CFL condition as it is implicit.*

Remark 3. *The kinetic Peterlin model (1) is equipped with the initial conditions (1e), from which we infer the following discrete initial values,*

$$\mathbf{u}_h^0 := \Pi_h^S[(\mathbf{u}_0, 0)]_1 \in V_h, \quad \psi_{h,N}^0(\cdot, \mathbf{R}) := \Pi_h \psi^0(\cdot, \mathbf{R}) \in X_h^1. \tag{20}$$

Here $\mathbf{u}_h^0$ is the first component of the Stokes projection $\Pi_h^S : V \times Q \to V_h \times Q_h$ of the couple $(\mathbf{u}^0, 0)$. By $\Pi_h : C(\bar{\Omega}) \to X_h^1$ we denote the Lagrange interpolation operator, cf., e.g., [15, Definition 1]. Further, we compute the values $\phi_{zk}^0(\mathbf{x}_i)$ for all $\mathbf{x}_i \in \mathcal{V}_h$ using the spectral decomposition (12).

2.5 Conservation of mass

The Hermite spectral method allows us to show the discrete counterpart of the conservation of mass with respect to the probability density function, which is one of the important features of the numerical scheme.

Theorem 2.2. (Discrete conservation of mass)
Let $\psi_{h,N} \in W_h \times \mathcal{P}_N^2$ be the solution of the multiscale scheme from Definition 3. Let the probability density function be such that $\psi(0, \mathbf{x}, \mathbf{R}) = \psi^0(\mathbf{R})$ and satisfies (1c). Then, for $n = 0, \dots, N_T$, it holds that

$$\int_{\mathfrak{D}} \psi_{h,N}^n(\mathbf{R})\, d\mathbf{R} = \int_{\mathfrak{D}} \psi^0(\mathbf{R})\, d\mathbf{R} = 1.$$

The proof of Theorem 2.2 comes after two preliminary lemmas.

Lemma 2.3.
Let the assumptions of Theorem 2.2 be satisfied. Then $\phi_{00}^n(\mathbf{x})$ is constant for all $\mathbf{x} \in \Omega$ and any time t^n.

Proof. The proof is done by induction for $n = 0, \dots, N_T - 1$.

- By the assumption of the lemma the coefficients ϕ_{zk}^0 are independent of $\mathbf{x}$. In particular, ϕ_{00}^0 is constant in Ω.
- Assume $\phi_{00}^n(\mathbf{x}) = \phi_{00}^n$ is a constant function in Ω. Then equation (18a) with (16) directly yields $\phi_{00}^*(\mathbf{x}_i) = \phi_{00}^n(\mathbf{x}_i) = \phi_{00}^n$. By Lax-Milgram theorem [12], equation (18b) has a unique solution ϕ_{zk}^{n+1}, for $z, k = 0, \dots, N$. We know that for $z = k = 0$ the constant ϕ_{00}^* is the solution, since $\phi_{00}^* \circ X_1^n = \phi_{00}^*$. Thus $\phi_{00}^{n+1}(\mathbf{x}) = \phi_{00}^* = \phi_{00}^n$. This concludes the proof.

□

We recall another useful property of weighted Hermite polynomials without the proof.

Lemma 2.4. [18, Lemma 4]
For the weighted Hermite polynomial $\tilde{H}_n(r)$ it holds that

$$\int_{\mathbb{R}} \tilde{H}_n(r)\, dr = 0, \ \textit{for } n \geq 1.$$

Proof of Theorem 2.2. The conservation of mass at the discrete level is a direct consequence of Lemmas 2.3 and 2.4. Indeed, we have

$$\begin{aligned}\int_{\mathfrak{D}} \psi^n_{h,N}(\mathbf{R})\, d\mathbf{R} &= \int_{\mathfrak{D}} \sum_{z,k=0}^{N} \phi^n_{zk} \tilde{H}_z(r_1)\tilde{H}_k(r_2)\, d\mathbf{R} = \int_{\mathfrak{D}} \phi^n_{00}\tilde{H}_0(r_1)\tilde{H}_0(r_2)\, d\mathbf{R} \\ &= \int_{\mathfrak{D}} \phi^0_{00}\tilde{H}_0(r_1)\tilde{H}_0(r_2)\, d\mathbf{R} = \int_{\mathfrak{D}} \sum_{z,k=0}^{N} \phi^0_{zk} \tilde{H}_z(r_1)\tilde{H}_k(r_2)\, d\mathbf{R} \\ &= \int_{\mathfrak{D}} \psi^0(\mathbf{R})\, d\mathbf{R},\end{aligned}$$

which concludes the proof. □

3 Numerical experiments

We present various numerical experiments in two space dimensions ($d = 2$) in order to demonstrate the performance of the proposed simulation method. We consider some classical benchmark problems from the ones with simple setting to the ones involving complex geometry. The complete multiscale solver is used in all subsequent experiments except the extensional flow in Subsection 3.1, in which only the configuration space solver on the unbounded domain is verified.

3.1 Extensional flow

Firstly, we test only the *configuration space solver* (18a). We consider an extensional flow, where the velocity field is fixed and given by $\nabla_x \mathbf{u} = \mathrm{diag}\{\kappa, -\kappa\}$ with the extension rate $\kappa = 0.5$. In this case it is possible to find the steady state solution of (1b). It reads

$$\psi_{\mathrm{ref}}(\mathbf{R}) = cM \exp\left\{\lambda \mathbf{R}^T \nabla_x \mathbf{u} \mathbf{R}\right\}, \quad M(\mathbf{R}) = \frac{1}{2\pi} \exp\left\{-\frac{1}{2}|\mathbf{R}|^2\right\},$$

where c is a normalization constant. In all subsequent tests we take the initial value $\psi^0(\mathbf{R}) = M(\mathbf{R})$. Note, that it satisfies the assumptions of Theorem 2.2. We can also compute the reference value of the macroscopic conformation tensor corresponding to the steady state distribution ψ_{ref}. Indeed, it reads

$$\mathbf{C}_{\mathrm{ref}} = \int_{\mathfrak{D}} (\mathbf{R} \otimes \mathbf{R}) \psi_{\mathrm{ref}}\, d\mathbf{R} = \begin{pmatrix} 2 & 0 \\ 0 & \frac{2}{3} \end{pmatrix}.$$

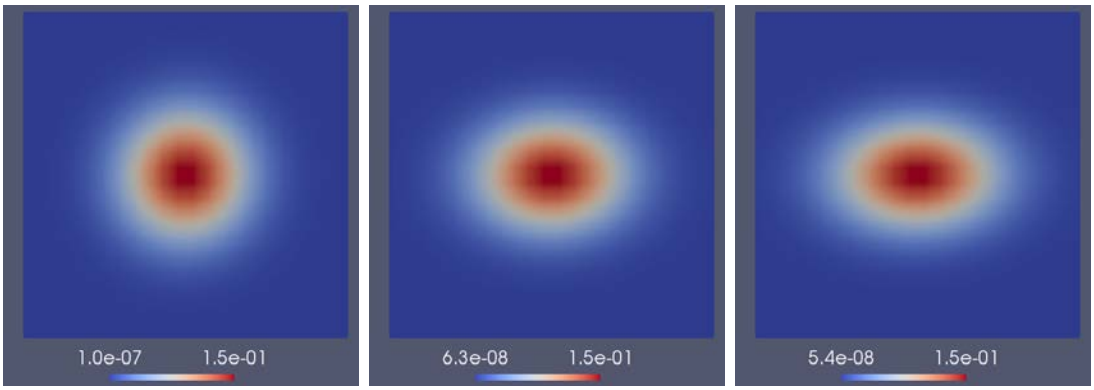

(a) t=0 (b) t=0.1 (c) t=1

(d) t=2 (e) t=10 (f) steady state

Figure 1: Extensional flow: time evolution of ψ towards the steady state, $N = 40$

Figure 1 depicts the time evolution of ψ towards the steady state ψ_{ref} for $N = 40$. The evolution of the three components of the symmetric conformation tensor is shown in Figure 2 together with the value of the integral of ψ over the configuration space $\mathfrak{D} = \mathbb{R}^2$ for different values of N till time $t = 10$. The corresponding relative errors of the probability density function in $L^2(\mathfrak{D})$-norm, and of the diagonal elements of the conformation tensor are listed in Table 1 below. We can clearly observe the experimental convergence of the solution with increasing polynomial degree N, and thus with an increasing number of the grid points $\mathbf{R}_{ij}$ in the discrete configuration space $\mathfrak{D}_N$.

Table 1: Extensional flow: numerical error

N	8	10	16	20	30
$\|\psi_h - \psi_{\text{ref}}\|_{L_2(\mathfrak{D})}$	2.1e-2	1.3e-2	3.3e-3	1.3e-3	1.5e-4
$\|C_{11} - C_{11\text{ref}}\|$	1.9e-1	7.9e-2	5.5e-3	8.8e-4	6.2e-5
$\|C_{22} - C_{22\text{ref}}\|$	8.6e-2	5.5e-3	2.2e-3	7.0e-5	1.0e-6

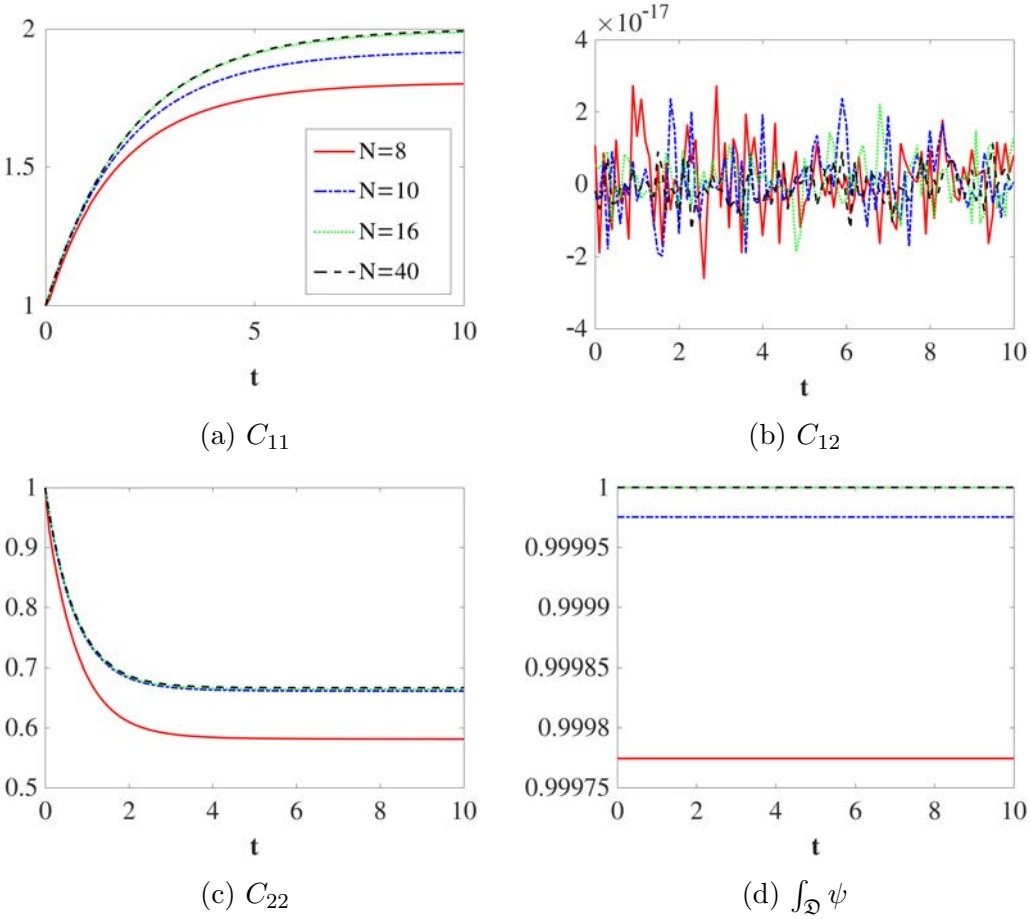

(a) C_{11} (b) C_{12}

(c) C_{22} (d) $\int_{\mathfrak{D}} \psi$

Figure 2: Extensional flow: time evolution till time $t = 10$

3.2 Poiseulle flow

In this experiment we test a periodic plane Poiseulle flow in computational domain $\Omega_h = [0, 1]^2$.The initial values are set as

$$(\mathbf{u}^0, \psi^0) = (\mathbf{u}_{ref}, M), \text{ with } \mathbf{u}|_{ref} = \big(x_2(1 - x_2), 0\big)^T.$$

In the horizontal direction we set the periodic boundary conditions for $\mathbf{u}$ and ψ. The upper and bottom boundaries are treated as no-slip walls with respect to the velocity. In addition, the homogeneous Neumann boundary condition is adopted for ψ on the latter boundaries. We set $\Delta t = h$, and the model parameters $\nu = 0.5$, $\lambda = 0.5$, $\varepsilon = 0$, $\Gamma(\mathrm{tr}\mathbf{C}) = \gamma(\mathrm{tr}\mathbf{C}) = 1$. The choice of ε, Γ and γ leads to the well-known Oldroyd-B model. This setting allows us to find the exact solution of the conformation tensor, i.e.,

$$C_{11} = 1 + 2\lambda \left|\frac{\partial u_2}{\partial x_2}\right|^2 \big(\lambda - (t + \lambda)e^{-t/\lambda}\big), \quad C_{12} = \lambda \frac{\partial u_2}{\partial x_2}(1 - e^{-t/\lambda}), \quad C_{22} = 1. \tag{21}$$

Figure 3 shows that the numerical solution coincides with the analytical values (21) computed at time $t = 10$. To further state the numerical convergence, we record

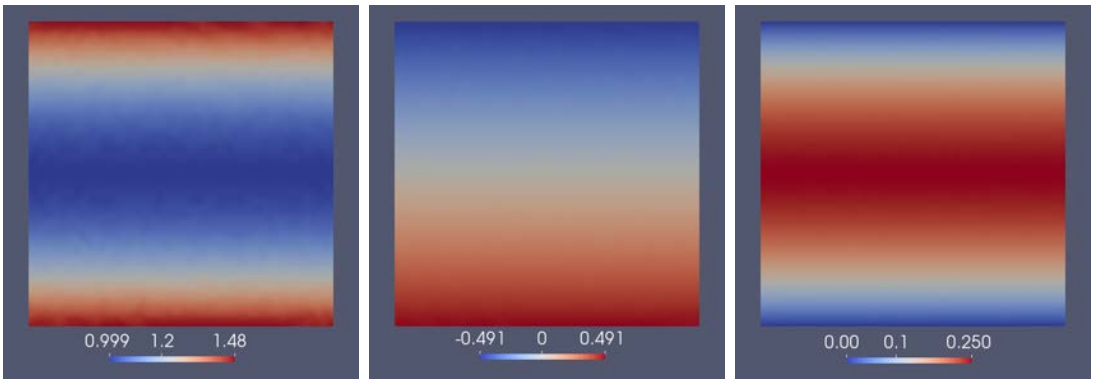

(a) C_{11} (b) C_{12} (c) u_1

Figure 3: Poiseulle flow: solution at time $t = 10$

the relative errors $e_v := v - v_{ref}$ for $v \in \{\mathbf{u}, C_{11}, C_{12}, C_{22}\}$. Table 2 indicates the numerical error is getting smaller both with an increasing mesh size h and increasing Hermite polynomial degree N.

Table 2: Poiseulle flow: numerical error at $t = 1$

$1/h$	N	$\|e_{\mathbf{u}}\|_{L^2}$	$\|e_{\mathbf{u}}\|_{H^1}$	$\|e_{C_{11}}\|_{L^2}$	$\|e_{C_{12}}\|_{L^2}$	$\|e_{C_{22}}\|_{L^2}$
16	8	2.15e-3	1.11e-2	3.17e-2	6.41e-2	2.82e-2
32	12	5.17e-4	4.33e-3	5.30e-3	1.45e-2	2.64e-3
64	16	1.30e-4	2.24e-3	2.58e-3	7.85e-3	1.53e-3

3.3 Driven cavity flow

For one of the benchmark problems for viscoleastic fluids, the driven cavity flow, we set $\Delta t = 0.05$, $\nu = 0.59$, $\varepsilon = 0$, $\lambda = 0.5$, and choose $\Gamma(\mathrm{tr}\mathbf{C}) = (\mathrm{tr}\mathbf{C})^2$, $\gamma(\mathrm{tr}\mathbf{C}) = 1$, which indeed covers a PTT model. The boundary condition for velocity is set as $\mathbf{u} = (16x_1^2(1-x_1)^2, 0)^T$ on the top boundary and zero otherwise. Figure 4 depicts the contour lines of pressure, the values of the velocity and the conformation tensor at $t = 2$. In Figure 5 we present the time evolution of the kinetic energy, the elastic energy of the polymers represented by the maximum and minimum of the trace of the conformation tensor, and the total mass of ψ.

3.4 Flow past cylinder

Now we present the performance of the multiscale solver for a flow past cylinder, a widely considered benchmark problem with a complex geometry. Note that our choice of parameters $\varepsilon = \lambda = \Gamma(\mathrm{tr}\mathbf{C}) = \gamma(\mathrm{tr}\mathbf{C}) = 1$ covers a diffusive Oldroyd-B model. The boundary conditions are the same as in the Poiseulle flow test and the

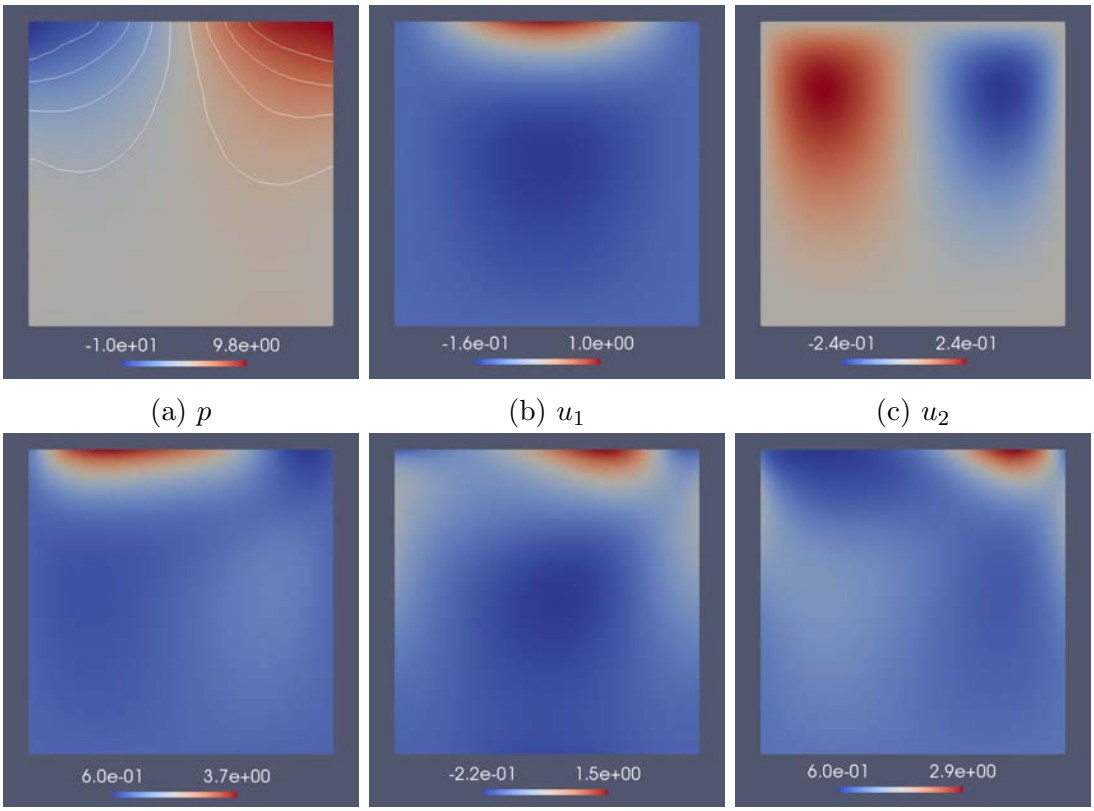

(a) p (b) u_1 (c) u_2

(d) C_{11} (e) C_{12} (f) C_{22}

Figure 4: Driven cavity flow: solution at time $t = 2$

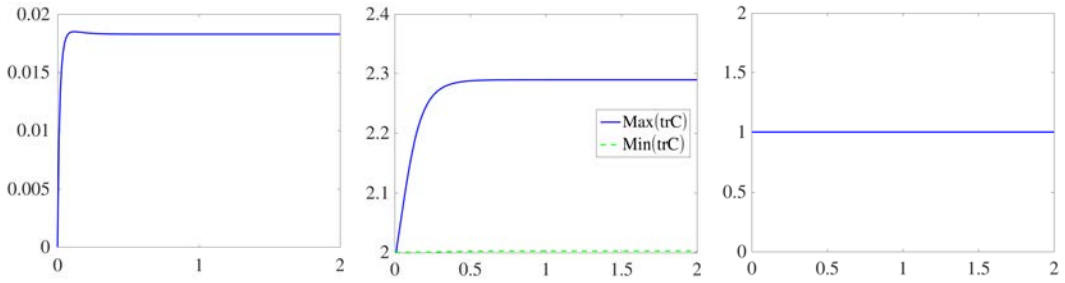

(a) kinetic energy (b) $\operatorname{tr} \mathbf{C}$ (c) $\int_{\Omega \times \mathfrak{D}} \psi$

Figure 5: Driven cavity flow: time evolution up to time $t = 4$

inlet velocity is $\mathbf{u} = \left(\frac{1}{4}x_2(1-x_2), 0\right)^T$. See Figure 6 for the numerical solution for $T = 4$, $\Delta t = 0.01, \nu = 0.59$.

Conclusion

We have proposed a multiscale scheme for numerical simulation of the unsteady motion of dilute polymer solutions with infinitely extensible molecules modelled by the incompressible Navier-Stokes-Fokker-Planck system. For the simulation

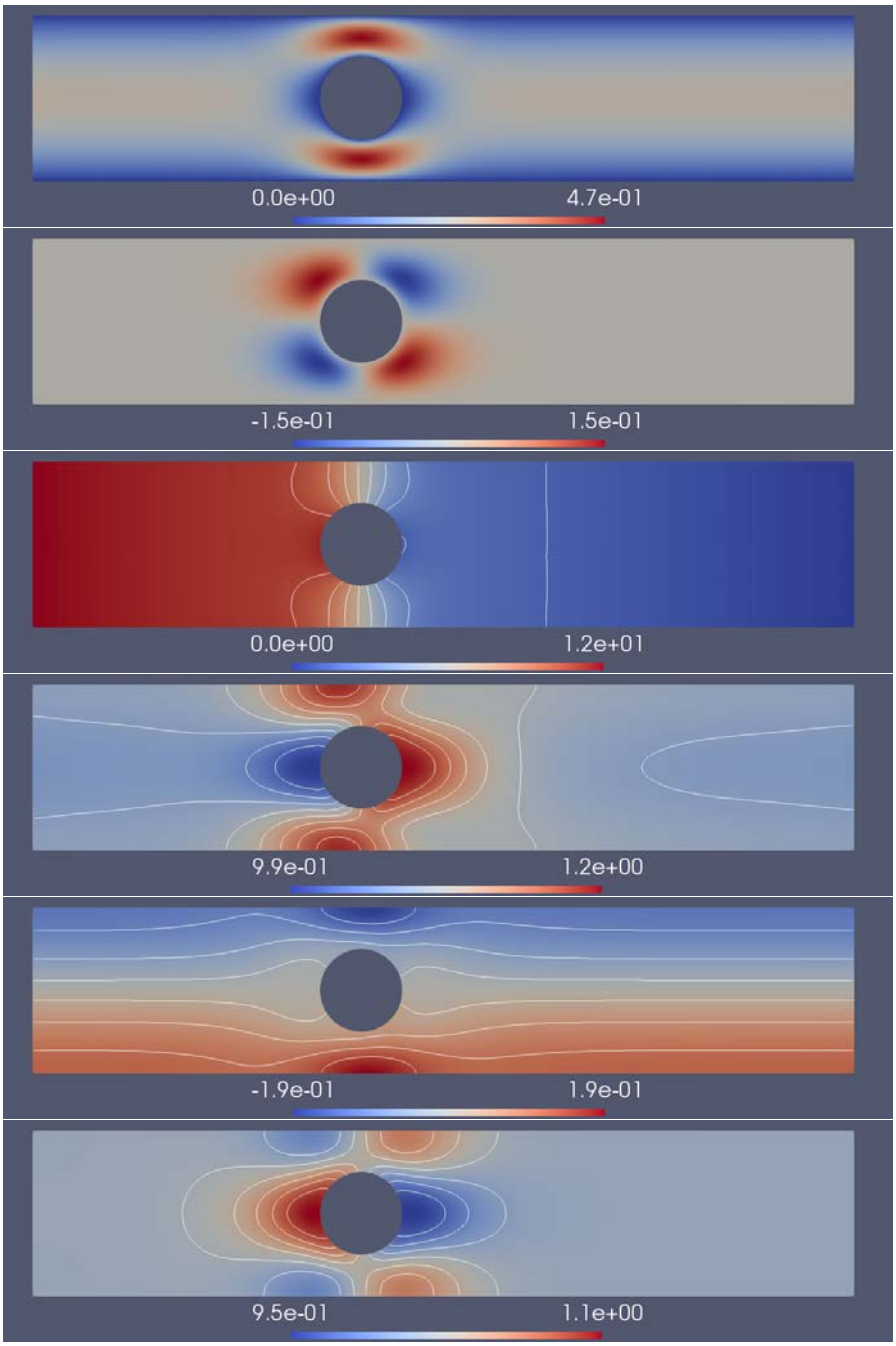

Figure 6: Flow past cylinder: from top to bottom are u_1, u_2, p, C_{11}, C_{12}, C_{22}

of the macroscopic solvent we used a stabilized Lagrange-Galerkin method. To solve the kinetic equation for the distribution of polymer molecules we split this equation into two parts; the first part in the physical space was solved by the Lagrange-Galerkin method, while the second part in infinite configuration space was approximated by the Hermite spectral method. We have proven that the scheme preserves mass with respect to the probability density. Demonstrating the performance of our solver, we have presented several numerical experiments,

from which we could conclude the numerical convergence for decreasing physical mesh size h and increasing number N of grid points in the discrete configuration space (degree of the Hermite polynomial) as well. The theoretical result on the discrete conservation of mass has been also confirmed by the numerical tests. To the best of our knowledge, this is the first result on the numerical simulation of dilute solutions with infinitely extensible polymers.

Acknowledgements

The research leading to these results has received funding from the European Research Council under the European Union's Seventh Framework Programme (FP7/2007-2013)/ ERC Grant Agreement 320078. The Institute of Mathematics of the Academy of Sciences of the Czech Republic is supported by RVO:67985840. The authors would like to thank Prof. Dr. M. Lukáčová-Medvid'ová (University of Mainz) for the fruitful discussions on this topic and Dr. K. Werth (University of Mainz) for his help with the code optimization.

References

[1] A. Abedijaberi and B. Khomami, *Continuum and multi-scale simulation of mixed kinematics polymeric flows with stagnation points: closure approximation and the high Weissenberg number problem.*, J. Non-Newton. Fluid Mech., 166 (2011), pp. 533–545.

[2] J.W. Barrett and E. Süli, *Existence and equilibration of global weak solutions to kinetic models for dilute polymers I: finitely extensible nonlinear bead-spring chains*, Math. Models Methods Appl. Sci., 21 (2011), pp. 1211–1289.

[3] J.W. Barrett and E. Süli, *Existence of global weak solutions to the kinetic Hookean dumbbell model for incompressible dilute polymeric fluids*, Nonlinear Anal-Real, 39 (2018), pp. 362–395.

[4] F. Brezzi and J. Pitkäranta, *On the stabilization of finite element approximations of the Stokes equations*, in Efficient Solutions of Elliptic Systems, W Hackbusch, ed., Vieweg, Wiesbaden, 1984, pp. 11–19.

[5] C. Chauvière and A. Lozinski, *Simulation of dilute polymer solutions using a Fokker–Planck equation*, Comput. Fluids, 33 (2004), pp. 687–696.

[6] P.G. Ciarlet, *The Finite Element Method for Elliptic Problems*, Studies in Mathematics and its Applications, Elsevier Science, 1978.

[7] P. Degond and H. Liu, *Kinetic models for polymers with inertial effects*, Netw. Heterog. Media, 4 (2009), pp. 625–647.

[8] J.C.M. Fok, B. Guo, and T. Tang, *Combined Hermite Spectral-Finite Difference Method for the Fokker-Planck Equation*, Math. Comput., 71 (2002), pp. 1497–1528.

[9] P. Gwiazda, M. Lukáčová-Medviďová, H. Mizerová, and A. Świerczewska-Gwiazda, *Existence of global weak solutions to the kinetic Peterlin model*, arXiv:, (2017).

[10] C. Helzel and F. Otto, *Multiscale simulations for suspensions of rod-like molecules*, J. Comput. Phys., 216 (2006), pp. 52–75.

[11] D.J. Knezevic and E. Süli, *A heterogeneous alternating-direction method for a micro-macro dilute polymeric fluid model*, ESAIM: M2AN, 43 (2009), pp. 1117–1156.

[12] P. D. Lax and A. N. Milgram, *Parabolic Equations*, in Contributions to the Theory of Partial Differential Equations, Lipman Bers, Salomon Bochner, and Fritz John, eds., vol. 33 of Annals of Mathematics, Princeton University Press, Berlin, Boston, 1955, ch. IX.

[13] A. Lozinski and C. Chauvière, *A fast solver for Fokker-Planck equation applied to viscoelastic flows calculations: 2D FENE model*, J. Comput. Phys., 189 (2003), pp. 607–625.

[14] M. Lukáčová-Medviďová, H. Mizerová, Š. Nečasová, and M. Renardy, *Global existence result for the Peterlin viscoelastic model*, SIAM J. Math. Anal., 49 (2017), pp. 2950–2964.

[15] M. Lukáčová-Medviďová, H. Mizerová, H. Notsu, and M. Tabata, *Numerical analysis of the Oseen-type Peterlin viscoelastic model by the stabilized Lagrange–Galerkin method, Part I: A nonlinear scheme*, ESAIM: M2AN, 51 (2017), pp. 1637–1661.

[16] M. Lukáčová-Medviďová, H. Mizerová, H. Notsu, and M. Tabata, *Numerical analysis of the Oseen-type Peterlin viscoelastic model by the stabilized Lagrange–Galerkin method, Part II: A linear scheme*, ESAIM: M2AN, 51 (2017), pp. 1663–1689.

[17] M. Lukáčová-Medviďová, H. Notsu, and B. She, *Energy dissipative characteristic schemes for the diffusive Oldroyd-B viscoelastic fluid*, Int. J. Numer. Methods Fluids, 81 (2016), pp. 523–557.

[18] M. Mohammadi and A. Borzi, *A Hermite spectral method for a Fokker-Planck optimal control problem in an unbounded domain*, Int. J. Uncertain. Quantif., 5 (2015), pp. 233–254.

[19] H. Notsu and M. Tabata, *Error estimates of a pressure-stabilized characteristics finite element scheme for the Oseen equations*, J. Sci. Comput., 65 (2015).

[20] H. Notsu and M. Tabata, *Error estimates of a stabilized Lagrange-Galerkin scheme for the Navier-Stokes equations.*, ESAIM: M2AN, 50 (2016), pp. 361–380.

[21] A. Peterlin, *Hydrodynamics of macromolecules in a velocity field with longitudinal gradient*, J. Polymer Sci. Part. B., Polymer Lett., (1966), pp. 287–291.

[22] J. Shen, T. Tang, and L. Wang, *Spectral methods. Algorithms, analysis and applications.*, Berlin: Springer, 2011.

[23] J. Shen and L. Wang, *Some Recent Advances on Spectral Methods for Unbounded Domains*, Commun. Comput. Phys., 5 (2009), pp. 195–241.

[24] J.D. Shieber, *Generalized Brownian configuration field for Fokker–Planck equations including center-of-mass diffusion*, J. Non-Newton. Fluid, 135 (2006), pp. 179–181.

[25] T. Tang, S. McKee, and M.W. Reeks, *A spectral method for the numerical solutions of a kinetic equation describing the dispersion of small particles in a turbulent flow*, J. Comp. Phys., 103 (1992), pp. 222 – 230.